

This discussion paper is/has been under review for the journal Atmospheric Chemistry and Physics (ACP). Please refer to the corresponding final paper in ACP if available.

Synoptically-induced variability in the microphysical properties of the South East Pacific stratocumulus deck

D. Painemal and P. Zuidema

Rosenstiel School of Marine and Atmospheric Sciences University of Miami, USA

Received: 4 November 2009 – Accepted: 14 November 2009 – Published: 27 November 2009

Correspondence to: D. Painemal (dpainemal@rsmas.miami.edu)

Published by Copernicus Publications on behalf of the European Geosciences Union.

ACPD

9, 25523–25564, 2009

Synoptic variability of the stratocumulus deck

D. Painemal and
P. Zuidema

Title Page

Abstract

Introduction

Conclusions

References

Tables

Figures



Back

Close

Full Screen / Esc

Printer-friendly Version

Interactive Discussion

Abstract

Synoptic variations associated with changes in satellite-derived cloud droplet number concentrations (N_d) for the southeast Pacific stratocumulus deck were examined using a composite analysis applied to daily values from the five October months of 2001, 2005, 2006, 2007 and 2008. MAX and MIN N_d composites were defined by the top and bottom terciles of daily area-mean N_d values over the Arica Bight, the region with the largest mean oceanic N_d . N_d and ship-based accumulation mode aerosol concentrations (N_a) correlate well ($r = 0.65$), with a best-fit aerosol activation value $\frac{d \ln N_d}{d \ln N_a}$ of 0.53 for pixels with $N_d > 50 \text{ cm}^{-3}$. The adiabatically-derived MODIS cloud depths also correlate well with the ship-based cloud depths ($r = 0.7$), though are consistently higher (mean bias of almost 60 m). The MAX- N_d composite is characterized by a weaker subtropical anticyclone and weaker winds both at the surface and the lower free troposphere than the MIN- N_d composite. The MAX- N_d composite clouds over the Arica Bight are thinner than the MIN- N_d composite clouds, have lower cloud tops, and occur within warmer, drier free tropospheres (as deduced from radiosondes) that imply greater coastal subsidence. The cloud thinning compensates radiatively for increased reflectance from increases in N_d , most apparent near the coast. CloudSat radar reflectivities do not imply significant aerosol scavenging by precipitation near the coast, indicating that variability in wind transport contributes to the aerosol variability. The co-occurrence of more boundary-layer aerosol/higher N_d within a more stable atmosphere suggests a boundary layer source for the aerosol, rather than the free troposphere.

Along 85° W , the top-of-atmosphere shortwave fluxes are significantly higher ($\sim 50\%$) for the MAX- N_d composite than for the MIN- N_d composite, with thicker clouds and higher cloud fractions. The change in N_d at this location is small (though positive), so that the composite difference primarily reflects synoptic changes. A one-point spatial correlation map reveals anomalous northerly winds at 850 hPa account for an anomalous warm temperature advection. The increase in the static stability along 85° W is highly correlated to the increased cloud fraction, despite accompanying weaker free

ACPD

9, 25523–25564, 2009

Synoptic variability of the stratocumulus deck

D. Painemal and
P. Zuidema

Title Page

Abstract

Introduction

Conclusions

References

Tables

Figures

⏪

⏩

◀

▶

Back

Close

Full Screen / Esc

Printer-friendly Version

Interactive Discussion

tropospheric subsidence. This synoptic impact on offshore cloud properties is arguably our most radiatively important finding, and draws attention to the free tropospheric meridional flow as a meteorological control.

1 Introduction

5 The subtropical cloud-capped marine boundary layer has a strong climate impact through the decks' high solar reflectivity whereas the emitted long-wave radiation remains close to that of surface emission under clear skies (Hartmann et al., 1992). A deeper understanding of the processes affecting the radiative properties of maritime warm clouds, both large-scale and microphysical, is necessary for developing confidence in future climate predictions. This is becoming particularly important as more aerosol indirect effects become incorporated into climate models. Currently only the cloud albedo effect ($\left. \frac{\partial A}{\partial N_d} \right|_{\text{lwp,met}}$, or the change in cloud albedo A with cloud droplet number N_d , all else held constant, Twomey, 1977), is considered in the Intergovernmental Panel on Climate Change (IPCC) 2007 assessment. Other effects, such as influences on the cloud albedo through changes in liquid water path (LWP) induced by changes in N_d ($\left. \frac{\partial A}{\partial(\text{lwp})} \frac{\partial(\text{lwp})}{\partial N_d} \right|_{\text{met}}$, this includes the cloud lifetime effect, Albrecht, 1989), are not yet formally included in the IPCC assessment. This acknowledges gaps in our understanding. Current IPCC estimates of a forcing of -1.2 W m^{-2} for the combined aerosol direct effect and cloud albedo effect alone already exceed an upper-bound residual estimate of -1.1 W m^{-2} for all aerosol direct and indirect effects combined from a recent observationally-derived energy balance (Murphy et al., 2009).

Examples of how higher aerosol loadings may not necessarily increase cloud reflectance include Matsui et al. (2006), who associate more aerosol with lower liquid water paths globally, and, similarly, Han et al. (2002). A tenet of the cloud lifetime effect, that higher LWPs are associated with longer cloud lifetimes, has also recently been called into question (Christensen et al., 2009). Theoretical and modeling support

Synoptic variability of the stratocumulus deck

D. Painemal and
P. Zuidema

Title Page

Abstract

Introduction

Conclusions

References

Tables

Figures



Back

Close

Full Screen / Esc

Printer-friendly Version

Interactive Discussion

for the observations has come from, among others, Jiang et al. (2002) and Ackerman et al. (2004), with more discussion in Stevens and Feingold (2009).

Dynamic compensation of aerosol indirect effects, through, for example, changes in the free troposphere conditions, draws attention to the need to control for meteorological forcings, a difficulty in both modeling and observational assessments of cloud-aerosol interactions. Otherwise, large-scale influences that affect both the aerosol and cloud properties can be mistaken as an aerosol influence on clouds. Atmospheric static stability is often chosen as a meteorological control variable, because static stability is known to correlate well with stratocumulus cloud fraction at seasonal scales (Klein and Hartmann, 1993). Matsui et al. (2006) then observed that cloud droplet sizes tend to be the smallest under strong inversions as well as within polluted environments. Mauger and Norris (2007) further examined the static stability of parcel back-trajectories of satellite-derived aerosol and cloud properties, and found that the covariation of aerosol amount and cloud fraction with static stability could be even more significant one to three days previous. Given the typically short time response of clouds to aerosols, however, it is unclear if static stability alone is sufficient as a meteorological control variable (e.g., Klein, 1997).

The southeast Pacific stratocumulus deck is one region where aerosol impacts on cloud microphysics are potentially significant, with Bennartz (2007) and Wood et al. (2008) showing large ($>200 \text{ cm}^{-3}$) cloud droplet number concentrations retrieved from MODerate resolution Imaging Spectroradiometer (MODIS) data along the Peru and Chile coast (17° S – 32° S). Though less clear from satellite imagery, measurements taken during the VAMOS Ocean-Coupled-Atmosphere-Land-Study (VOCALS) Regional Experiment provides evidence of anthropogenic emissions as far west as 85° W (Hawkins et al., 2010). Bennartz (2007) speculated that the downwind transport of polluted air affected the microphysics of these clouds. Huneus et al. (2006) hypothesized instead that entrainment of polluted air from the free troposphere could be responsible for the N_d increases. These conflicting hypotheses arise because the Andes Cordillera influences how aerosol can interact with the stratocumulus deck. Al-

Synoptic variability of the stratocumulus deck

D. Painemal and
P. Zuidema

Title Page

Abstract

Introduction

Conclusions

References

Tables

Figures

◀

▶

◀

▶

Back

Close

Full Screen / Esc

Printer-friendly Version

Interactive Discussion

though the Andes protect the deck from routine aerosol-laden continental outflow, high-altitude copper smelters emit sulfate aerosols above the marine boundary layer. The Andes also dictate along-shore winds both at the surface and the lower free troposphere, in principal transporting aerosol from the more developed southern regions to the north. Orography affects the boundary layer depth and increases the difficulty of modeling regional aerosol-cloud interactions accurately, increasing the value of observational analyses (e.g., Zuidema et al., 2009; Wyant et al., 2009).

Holistic regional assessments relying on satellite data, available local data, and re-analyses, such as presented here, can provide a benchmark for modeling efforts with similar goals. In this study, we focus further on the synoptic and microphysical variability of the southeast Pacific stratocumulus region, and attempt to deconvolve the local synoptic impacts on cloud properties from those that are influenced by aerosol variability. Our goal is to address the following questions: 1) what is the meteorology associated with N_d variability? 2) Do N_d increases correspond to an enhanced cloud albedo? 3) Do atmospheric conditions favor aerosol incorporation into the cloud through free-tropospheric subsidence, or from within the boundary layer?

We use NCEP/NCAR Reanalysis to depict the large-scale circulation, and assume it is accurate except near the coast, where we also rely on radiosonde data. Cloud properties are derived primarily from MODIS data. Frequently overcast skies, relatively homogenous cloud conditions, and favorable sun-satellite viewing geometries aid the retrievals. Cloud droplet numbers retrieved from satellite serve as an aerosol proxy, taking advantage of frequently overcast skies that make satellite retrievals of clear-sky aerosol properties and its issues (e.g., Loeb and Schuster, 2008) a moot point. The physical connection between aerosol and N_d is justified further through comparisons between ship-based aerosol measurements and the satellite retrievals. A composite analysis is then applied to five October months of daily data. This month corresponds to the regional climatological maximum of the Sc deck (Klein and Hartmann, 1993), and the focus on October months alone is intended to minimize influences from the seasonal progression. An underlying premise is that the differences in cloud properties

Synoptic variability of the stratocumulus deck

D. Painemal and
P. Zuidema

Title Page

Abstract

Introduction

Conclusions

References

Tables

Figures

⏪

⏩

◀

▶

Back

Close

Full Screen / Esc

Printer-friendly Version

Interactive Discussion

associated with the largest differences in N_d are likely to reflect synoptic influences, rather than the effect of cloud-aerosol interactions. Our approach complements more thorough single case studies such as Huneeus et al. (2006) and provides a context for analyses of VOCALS Regional Experiment (VOCALS-Rex, Wood and Mechoso, 2008) data. We selected four October months coincident with NOAA research cruises (2001, 2005, 2006 and 2007), while October 2008 coincides with the VOCALS Regional Experiment. The dataset, methodology, and ship-satellite comparisons are detailed in Sect. 2, composite results are described in Sect. 3, the regional circulation is discussed in Sect. 4, precipitation characteristics in Sect. 5, and concluding remarks in Sect. 6.

2 Data and methods

We combined MODIS Collection 5 cloud effective radius (r_e) and cloud optical thickness (τ) retrievals (Platnick et al., 2003) to produce values for N_d and cloud depth (H_{sat}), and used a temperature threshold of 273 K to select for warm, liquid-only clouds. Instantaneous swath data (level 2) from both the Terra and Aqua platforms ($\sim 10:30$ LT and $\sim 13:30$ LT overpasses, respectively) were used for the validation comparisons shown in Sect. 2.2. These comparisons draw on a more comprehensive database of in-situ observations from six NOAA cruises (October, 2001, 2005, 2006, 2007, and November, 2003 and December, 2004). In contrast the composite analysis relies on daytime Terra level 3 data at $1^\circ \times 1^\circ$ spatial resolution for only the October months. At this latitude, the daily-mean values for each platform are effectively regrided individual swath data. The daytime Terra overpass was previously found to be the overpass most representative of daily-mean conditions (Zuidema et al., 2009). MODIS cloud top temperatures, derived from separate day and nighttime $11 \mu\text{m}$ equivalent brightness temperatures, were used to estimate a satellite cloud top height, and rely on a depth-varying lapse rate inferred from the cruise radiosondes (Zuidema et al., 2009). These are shown to capture daily synoptic-scale variations reasonably well within Painemal et al. (2009).

Synoptic variability of the stratocumulus deck

D. Painemal and
P. Zuidema

Title Page

Abstract

Introduction

Conclusions

References

Tables

Figures



Back

Close

Full Screen / Esc

Printer-friendly Version

Interactive Discussion



**Synoptic variability
of the stratocumulus
deck**D. Painemal and
P. Zuidema

[Title Page](#)[Abstract](#)[Introduction](#)[Conclusions](#)[References](#)[Tables](#)[Figures](#)[⏪](#)[⏩](#)[◀](#)[▶](#)[Back](#)[Close](#)[Full Screen / Esc](#)[Printer-friendly Version](#)[Interactive Discussion](#)

Estimates of the shortwave fluxes (SW) at the top of the atmosphere were obtained from the Clouds and Earth's Radiant Energy System (CERES, Wielicki et al., 1996) instrument on board the Terra platform. The CERES data allow a net radiative assessment of the combined microphysical and macrophysical changes that is somewhat independent of plane-parallel theory. We used the radiometric measurements from the shortwave channel (0.3–5 μm), and spatially averaged Single Scanner Footprint data to a $1^\circ \times 1^\circ$ spatial resolution. These data were only available for October 2001, 2005, and 2006. The occurrence of precipitation was determined from CloudSat radar reflectivity data (the Cloud-Geometrical-Profile product; Stephens et al., 2002) from October 2006, 2007 and 2008. Surface winds were provided by the satellite scatterometer QuikSCAT at a $0.25^\circ \times 0.25^\circ$ resolution; we only used the evening pass (18:00 LT) data. Non-satellite data sources are the NCEP/NCAR reanalysis (Kalnay et al., 1996) meteorological fields, with a horizontal resolution of $2.5^\circ \times 2.5^\circ$, and daily radiosonde observations at Antofagasta (23.43° S, 70.43° W, 120 a.m.s.l.) at 12:00 UTC (08:00 LT).

2.1 Basic relationships

MODIS retrievals of cloud optical depth and effective radius are routinely available, but small droplet sizes do not unambiguously indicate aerosol loading, because r_e is also a function of distance above cloud base (e.g., Schuller et al., 2003). Instead, we estimated N_d and H_{sat} from a combination of r_e and τ assuming adiabatic conditions (e.g. Bennartz, 2007; Szczodrak et al., 2001). This allows a separation of macrophysical and microphysical cloud property measures, and in addition facilitates a comparison to the ship-based measurements of N_a and H_{ship} .

The aerosol number concentration N_a is a direct measurement. We typically rely on data from a Particle Measuring System Lasair-II instrument, which measures all particles greater than 0.1 microns, but does not control for humidity. For the 2004 cruise, data from a Differential Mobility Analyser are used (Tomlinson et al., 2006). Aerosol counts gathered from both instruments during the 2003 cruise show good agreement (Tomlinson et al., 2006). In contrast, the ship-board cloud depths are estimated from

Synoptic variability of the stratocumulus deck

D. Painemal and
P. Zuidema

Title Page

Abstract

Introduction

Conclusions

References

Tables

Figures

⏪

⏩

◀

▶

Back

Close

Full Screen / Esc

Printer-friendly Version

Interactive Discussion

a ceilometer cloud base and inversion-derived cloud top. Such a comparison builds on previous assessments showing good correspondence between liquid water paths (LWPs) derived from MODIS data using the adiabatic approximation ($LWP = \frac{5}{9} \rho_w r_e \cdot \tau$; ρ_w is the density of the liquid water) and satellite microwave-derived values for overcast marine stratocumulus (e.g., Borg and Bennartz 2007; Seethala and Horvath, 2009).

A satellite-derived cloud depth H_{sat} also invokes the adiabatic lapse rate for liquid water content, Γ_{ad} . Evaluation of sounding-derived values for Γ_{ad} reveal that the lower, warmer coastal clouds have typical values between $2.1\text{--}2.3 \times 10^{-3} \text{ g m}^{-4}$, while clouds west of 75° W have values of $1.8\text{--}2.0 \times 10^{-3} \text{ g m}^{-4}$. Near-coastal liquid water content profiles in VOCALS-REx aircraft data often show diminished values near cloud top because of cloud top entrainment, which reduces the effective Γ_{ad} , while profiles from further offshore are close to adiabatic (see also Zuidema et al., 2005). With this in mind, we rely on a constant Γ_{ad} value of $2.0 \times 10^{-3} \text{ g m}^{-4}$, and approximate its uncertainty at 10%. H_{sat} is then estimated from the adiabatically-derived LWP using $LWP = \frac{\Gamma_{ad} H_{\text{sat}}^2}{2}$ as

$$H_{\text{sat}} = \sqrt{\frac{2}{\Gamma_{ad}} \frac{5}{9} \rho_w \cdot r_e \cdot \tau} \quad (1)$$

and cloud droplet concentration through

$$N_d = \Gamma_{ad}^{1/2} \frac{10^{1/2}}{4\pi \rho_w^{1/2} k} \cdot \frac{\tau^{1/2}}{r_e^{5/2}} \quad (2)$$

following Szczodrak et al. (2001). The parameter k corresponds to the ratio between the volume mean radius and the effective radius and is assumed constant at 0.8.

For overcast, opaque, mostly unbroken, warm cloud pixels, the error in H_{sat} from its input variables is $\sim 12\%$, after also assigning τ and r_e errors of $\sim 10\%$ (Bennartz, 2007; Platnick et al., 2003). The error in N_d will be dominated by the error in the MODIS-derived effective radius though the $r_e^{-5/2}$ dependence. The effective radius retrieval is

most suspect in broken cloud conditions, where r_e can be systematically overestimated (e.g., Marshak et al., 2006). We observed that low N_d values tended to be associated with high-LWP clouds (not shown), which are more likely to precipitate and be inhomogeneous, and also observed a poor correspondence to the surface-based aerosol measurements for the lower values of N_d (e.g., Fig. 1b). We attempt to minimize the impact of cloud inhomogeneities upon the N_d retrieval by limiting our quantitative analysis to N_d values $>50 \text{ cm}^{-3}$ for overcast (or nearly so) pixels. We estimate the error in this N_d subsample at 25% based on the input errors in τ , r_e and Γ_{ad} . This is less conservative than the uncertainty estimate of 50% within Bennartz (2007), but is justified by our more restricted, regional dataset.

2.2 Satellite-ship comparisons

H_{sat} and N_d derived from instantaneous level 2 data were spatially averaged over an area of 25 km by 25 km, corresponding to a 7 m s^{-1} “frozen turbulence” advective speed over one hour. The ship-based cloud depth (H_{ship}) is computed as the difference between the radiosonde inversion base height (placed at the temperature minimum; radiosondes were launched at either 4 or 6 h intervals) and hourly-averaged ceilometer cloud base heights. Comparisons were restricted to the one-hour time periods spanning the radiosondes.

H_{sat} and H_{ship} values correlate well with each other ($r = 0.54$), increasing to 0.7 when restricting the sample to $H_{\text{ship}} < 400 \text{ m}$ and to overcast periods (ceilometer hourly cloud fractions $>90\%$) (Fig. 1a; only overcast periods are shown). H_{sat} values often exceed H_{ship} , with a mean bias of 59 m for $H_{\text{ship}} < 400 \text{ m}$, seemingly indicating superadiabatic LWPs. Schuller et al. (2003) also found a similar bias between remote sensed and in-situ cloud depth; an explanation is currently lacking. Further cloud depth values shown here rely on Eq. (1) as given and do not correct for this bias.

Satellite-derived N_d are compared to ship-based aerosol concentrations (size $>0.1 \text{ micron}$) in Fig. 1b, with no constraint placed on the hourly ceilometer

Synoptic variability of the stratocumulus deck

D. Painemal and
P. Zuidema

Title Page

Abstract

Introduction

Conclusions

References

Tables

Figures

⏪

⏩

◀

▶

Back

Close

Full Screen / Esc

Printer-friendly Version

Interactive Discussion

cloud fractions towards increasing the data sample. Most of the aerosol concentration measurements were taken near 85° W and 20° S, with a limited sampling near the coast. N_d and N_a show an obvious correlation ($r = 0.65$, increasing to 0.8 for hourly-mean ceilometer cloud fractions >0.9), with N_d typically $< N_a$, demonstrating physical consistency. The values of both N_d and N_a are higher when sampled closer to the coast (east of 80° W, black filled circles in Fig. 1b).

A quantitative assessment of the observed $N_d - N_a$ relationship can be done through its measure of aerosol activation, expressed through an aerosol cloud index $\frac{d \ln N_d}{d \ln N_a}$ (McComiskey et al., 2009). We restrict the data samples to $N_d > 50 \text{ cm}^{-3}$ as a proxy for non-precipitating clouds and to control for overestimates in the effective radius retrievals caused by cloud inhomogeneities. We find a best-fit value for $\frac{d \ln N_d}{d \ln N_a}$ of 0.53. For comparison, Pruppacher and Klett (1997) suggest a value of 0.7 for $\frac{d \ln N_d}{d \ln N_a}$ based on droplet activation theory, while McComiskey et al. (2009) find an empirical value of 0.48 using cloud microphysical retrievals from surface-based remote sensors of marine stratocumulus clouds at Pt. Reyes, CA. Quaas et al. (2009) find a sensitivity of MODIS-derived N_d to the aerosol optical depth at Pt. Reyes that is close to the corresponding surface-based value.

Comparison to other published values of $\frac{d \ln N_d}{d \ln N_a}$ must take many factors into account. McComiskey et al. (2009) document a strong reduction with increasing scale, for example. Nevertheless, our value is fairly high despite the field-of-view differences and the large scale. Moreover, 42% of our variation in N_d is explained by the aerosol concentration variability, compared to 15% for McComiskey et al. (2009). Some of the explanation is provided by Fig. 2, for which daily maps of Terra N_d and LWP values were averaged over the five October months. Many of the higher N_d values are associated with thinner clouds ($\text{LWP} < 90 \text{ g/m}^2$, contours in Fig. 2) that are less likely to be drizzling (e.g., Leon et al., 2008) and more likely to be adiabatic if offshore (e.g., Zuidema et al., 2005). For such clouds, values of $\frac{d \ln N_d}{d \ln N_a}$ are typically higher (McComiskey et al., 2009; Kim et al., 2008). Three-dimensional radiative transfer effects upon the r_e and

Synoptic variability of the stratocumulus deck

D. Painemal and
P. Zuidema

[Title Page](#)[Abstract](#)[Introduction](#)[Conclusions](#)[References](#)[Tables](#)[Figures](#)[⏪](#)[⏩](#)[◀](#)[▶](#)[Back](#)[Close](#)[Full Screen / Esc](#)[Printer-friendly Version](#)[Interactive Discussion](#)

thereby Nd retrieval, which will be more pronounced for thicker, more broken clouds with naturally higher r_e , may also contribute to a higher value for $\frac{d \ln N_d}{d \ln N_a}$ by artificially lowering low values of N_d even further.

3 Observational composites

5 The instantaneous satellite-ship comparisons of cloud depth and cloud droplet number in Sect. 2, and for satellite-derived cloud top heights within Zuidema et al. (2009), provide confidence in the ability of the MODIS retrievals to represent the stratocumulus macro- and microphysics. The random error is further reduced by averaging over many samples within the composite. Our composite analysis is based on the
10 Terra-daytime-overpass, one degree spatial resolution (level 3) N_d variability over the apparently most-polluted region, the Arica Bight, defined here to span 71.5° W– 75.5° W and 18.5° S– 25.5° S (box in Fig. 2). Only scenes deemed overcast over the Arica Bight were used, defined through at least 70% overcast satellite pixels. Such overcast days occurred on 77% (120 days) of the total days. As seen in Fig. 2, mean LWP values are
15 small ($<70 \text{ g m}^{-2}$) over the region with the largest N_d .

Days are composited by the spatial-mean $\overline{N_d}$ over the Arica Bight into the MAX ($\overline{N_d} > 215.8 \text{ cm}^{-3}$) and MIN ($\overline{N_d} < 161.6 \text{ cm}^{-3}$) highest and lowest terciles of total overcast days (40 and 42 each) respectively. For the October, 2008, VOCALS-REx time period, the NCAR C-130 research flights RF01 and RF02 (15 and 18 October) occurred within
20 the only MAX composite case lasting six days, and RF03 occurred one day later (21 October). C-130 research flights RF04 (23 October), RF05 (25 October), and RF06 (28 October) were within one day of MIN- N_d composite days, and RF07 (31 October) coincided with a MIN- N_d composite day. Of the Twin Otter flights, the first three (16, 18, and 19 October) coincided with MAX cases, and the 24 and 29 October flights
25 coincided with MIN cases.

Synoptic variability of the stratocumulus deck

D. Painemal and
P. Zuidema

[Title Page](#)[Abstract](#)[Introduction](#)[Conclusions](#)[References](#)[Tables](#)[Figures](#)[⏪](#)[⏩](#)[◀](#)[▶](#)[Back](#)[Close](#)[Full Screen / Esc](#)[Printer-friendly Version](#)[Interactive Discussion](#)

MAX-MIN N_d composite differences (Fig. 3, colors) are a maximum by construction between 18°S – 27°S with values higher than 120 cm^{-3} , and a westward extension of about 8° . The climatological-mean N_d values are a maximum further north near 20°S , but the changes are smaller. Cloud droplet number concentrations along the Peruvian coast (north of 15°S) are slightly higher within the MIN- N_d composite than the MAX- N_d composite (negative values in Fig. 3). Near Antofagasta (23.43°S ; small black square) the N_d changes reach their maximum value of 160 cm^{-3} . MAX-MIN N_d composite differences in LWP reveal decreased LWPs east of 85°W ($\sim 20\text{ g m}^{-2}$) during the MAX- N_d composite, along with increased LWPs (10 – 30 g m^{-2}) west of 85°W (Fig. 3).

Time series of surface winds, cloud top heights, and geopotential height indicate the synoptic timescale of MAX/MIN N_d composite days and anticipate general differences (Fig. 4). Mean surface wind speeds (20°S – 30°S , 70°W – 100°W), mean cloud top heights alongshore (20°S – 30°S , 70°W – 80°W), and mean offshore 500 hPa geopotential height (15°S – 35°S , 70°W – 100°W , approximately the location of the climatological anticyclone) are shown along with the occurrence of MAX (dark triangles) and MIN (open triangles) N_d days. About one-half (two-thirds) of the MIN/MAX N_d days occur in groups of three or more days. MAX N_d days are more likely to be associated with weaker winds (Fig. 4a), shallower coastal boundary layers (Fig. 4b) and enhanced offshore mid-tropospheric geopotential heights (Fig. 4c). This synoptic grouping and its variability is further evident in Fig. 5: MAX (MIN) N_d days co-occur with weaker (stronger) coastal winds and lower (higher) cloud tops near shore. Some interannual variability is evident as well, with more MIN N_d cases occurring during 2007, coinciding with a weak cool ENSO phase, and more MAX N_d cases than MIN N_d cases occurring during 2001 and 2008, when more intense observational campaigns, the Eastern Pacific Investigation of Climate (Bretherton et al., 2004) and VOCALS-REx, visited the region.

**Synoptic variability
of the stratocumulus
deck**D. Painemal and
P. Zuidema

Title Page

Abstract

Introduction

Conclusions

References

Tables

Figures

⏪

⏩

◀

▶

Back

Close

Full Screen / Esc

Printer-friendly Version

Interactive Discussion

3.1 Satellite

The regional circulation patterns associated with each composite are shown in Fig. 6 (panels a and b, respectively). The anticyclone is strengthened offshore (85° W– 95° W) during the MIN N_d composite, with stronger surface winds and a strengthened coastal jet near 33° S (Fig. 6b). Surface winds are light within both composites at the northern end of the Arica Bight, where changes in N_d are also modest. Mean October values along with MAX-MIN N_d composite difference values are shown for the MODIS-derived cloud top height (Fig. 6c), cloud depth (Fig. 6d), cloud fraction (Fig. 6e), and top-of-atmosphere CERES shortwave fluxes (Fig. 6f). These reveal shallower boundary layer depths for the MAX N_d composite, by 200 m to 350 m, over a broad domain extending beyond the Arica Bight (Fig. 6c). Over the Arica Bight and along 80° W, these changes are associated with thinner clouds for the MAX N_d composite (Fig. 6d), by up to 50 m. West of 80° W, the pattern reverses, and clouds are slightly thicker for the MAX N_d composite than for the MIN N_d composite.

The mean MODIS cloud fraction is a maximum parallel to the Peruvian coast (contours, Fig. 6e), with the mean values in the top-of-atmosphere shortwave fluxes following a similar spatial pattern (Fig. 6f). The composite differences show that cloud fractions are diminished by about 5% over the Arica Bight for the MAX composite relative to the MIN composite, remain approximately the same off the coast of Peru, and increase significantly elsewhere – by up to 20% near 85° W, 25° S. The variation in the top-of-atmosphere shortwave fluxes (Fig. 6f) are broadly consistent with the cloud fraction changes. Over the Arica Bight, the MAX-MIN composite change in top-of-atmosphere SW fluxes is negative near the coast, and increases 500 km offshore. This reflects the compensation between increased brightening due to a higher N_d , and decreased brightening from a thinner cloud. Near the coast the cloud thinning ends up dominating radiatively, while further offshore the small increase in N_d is more radiatively important. The mean change over the Arica Bight region, defined by the box in Fig. 2, is 20 W m^{-2} , or an approximately 15% increase in the regional-mean cloud

Synoptic variability of the stratocumulus deck

D. Painemal and
P. Zuidema

Title Page

Abstract

Introduction

Conclusions

References

Tables

Figures



Back

Close

Full Screen / Esc

Printer-friendly Version

Interactive Discussion

albedo. Further south, the increase in cloud fraction over the Chilean coastal jet for the MAX N_d composite corresponds with an increase of approximately 50 W m^{-2} in the top-of-atmosphere shortwave fluxes, but over a region with small mean cloud fraction. The most dramatic changes in the fluxes are observed away from Arica Bight along 85° W , however, and are primarily associated with cloud fraction differences, with only small changes in the cloud droplet numbers.

3.2 Radiosonde

Composites of radiosondes from Antofagasta (23.43° S , 70.43° W ; 12:00 UTC or 08:00 LT) help us interpret the satellite composites near the location of maximum N_d variability (Fig. 7). This is particularly valuable because the NCEP/NCAR Reanalysis is deemed less reliable near the South American coastline. At the Antofagasta location, the MAX N_d composite satellite-derived cloud top heights are lower, the cloud are thinner, and the MODIS cloud fraction is decreased. The changes at Antofagasta are broadly representative of the Arica Bight region (Fig. 6). The radiosonde temperature profiles confirm that the MAX N_d cases are typically associated with a shallower boundary layer (Fig. 7a, solid black line). The main difference between the profiles occurs in the free troposphere, with the MAX N_d radiosonde composite possessing a warmer, drier free troposphere than the MIN N_d composite.

The implication of increased subsidence for the MAX N_d composite is supported by the structure of the observed zonal winds. While the zonal winds are weak for both cases, offshore easterlies above the inversion are slightly stronger for the MAX composite (Fig. 7c, solid lines), consistent with increased subsidence and divergence at the inversion. The corresponding Reanalysis profiles, shown for a location approximately 500 km offshore, depict the boundary layer weakly. The vertical placement of the temperature and moisture inversion is approximately correct, but the underestimate of the inversion strength is pronounced, so that the response of the zonal winds to the presence of the boundary layer is not captured correctly. In contrast to the temperature and moisture Reanalysis composite profiles, the sense of the change between the

Synoptic variability of the stratocumulus deck

D. Painemal and
P. Zuidema

Title Page

Abstract

Introduction

Conclusions

References

Tables

Figures



Back

Close

Full Screen / Esc

Printer-friendly Version

Interactive Discussion



MAX and MIN Reanalysis N_d zonal wind composites differs from the radiosonde composites, with greater offshore lower-tropospheric flow for the MIN Reanalysis composite, while the radiosondes show greater offshore lower-tropospheric flow for the MAX composite.

4 Regional circulation

The synoptic conditions associated with the two composites provides insight into the spatial extent of the subsidence changes identified in the radiosonde composites, and into the cloud property changes shown in Figs. 2–7. The important meteorological parameters governing stratocumulus cloud behavior at daily/synoptic time scales are not well-established (e.g., Klein, 1997; Zhang et al., 2009), although Reanalysis lower tropospheric stability is an often-used proxy (e.g., Mauger and Norris, 2007; Matsui et al., 2006). Here we defined the static stability through the difference between potential temperature (θ) at 850 hPa and 1000 hPa. This estimate was found to correlate better with MODIS cloud fraction than a static stability difference based on $\theta_{700\text{hPa}}$, as can be intuited from Fig. 7a. A spatial map of the correlation at daily time scales between $\theta_{850\text{hPa}} - \theta_{1000\text{hPa}}$ and MODIS cloud fraction (Fig. 8) shows the highest positive correlation at 85°W and 25°S ($r = 0.55$), which is higher than that reported for the northeast Pacific at 30°N , 140°W using $\theta_{700\text{hPa}} - \theta_{\text{surface}}$ ($r = 0.22$; Klein, 1997). The correlation is insignificant over the Arica Bight, also expected based on Fig. 7.

Figure 9 shows mean values of $\theta_{850\text{hPa}} - \theta_{1000\text{hPa}}$ (contours) along with the composite differences (greyscale). Higher mean static stabilities occur approximately where mean MODIS cloud fractions (Fig. 6e) are higher. The largest static stability difference between the two composites occurs near the southern boundary of the stratocumulus deck, at approximately 30°S , $75\text{--}77^\circ\text{W}$, near if slightly east of the highest composite differences in cloud fraction (Fig. 6e). The stability changes are large in the same general area where the correlation between cloud fraction and static stability is high (Fig. 9), rationalizing the choice of static stability for a synoptic analysis of this region.

Synoptic variability of the stratocumulus deck

D. Painemal and
P. Zuidema

Title Page

Abstract

Introduction

Conclusions

References

Tables

Figures



Back

Close

Full Screen / Esc

Printer-friendly Version

Interactive Discussion



**Synoptic variability
of the stratocumulus
deck**D. Painemal and
P. Zuidema

Title Page

Abstract

Introduction

Conclusions

References

Tables

Figures

⏪

⏩

◀

▶

Back

Close

Full Screen / Esc

Printer-friendly Version

Interactive Discussion

One approach to identifying meteorological influences on cloud-aerosol interactions is to use back-trajectories (e.g., Mauger and Norris, 2007), but these are fraught for the southeast Pacific by the poor reanalysis representation of the coastline. Instead, we performed a one-point linear correlation analysis using the 850 hPa temperature time series at 20° S and 75° W as the reference point (Fig. 10 filled square; note this is approximately 300 km west of the Twin Otter point Alpha destination during VOCALS-REx). This essentially substitutes $\theta_{850\text{hPa}}$ variability for the static stability variability at short time scales, justified by the strong influence of the sea surface temperature upon $\theta_{1000\text{hPa}}$. The 850 hPa temperature time series at 20° S and 75° W was correlated with the 850 hPa geopotential height, subsidence and wind field time series at all other reanalysis grid points (Fig. 10). The one-point correlation analysis reveals an anomalous trough to the west of South America, with enhanced subsidence near the coast and weakened subsidence offshore. Increases in the 850 hPa geopotential height between 75°–85° W are associated with anomalous northerly winds allowing the 850 hPa temperature to increase (i.e., free tropospheric cold temperature advection from the south is reduced), elevating the static stability and increasing cloud coverage. An example of the opposite behavior is discussed in Wyant et al. (2009) for mid-October, 2006, when enhanced southerly winds above the inversion corresponded to a decrease in cloud coverage and increase in a boundary-layer deepening at 85° W, 20° S. Apparent in Fig. 10 is that the disturbances are associated with mid-latitude intrusions as opposed to equatorial intrusions, with the composite analysis preferentially selecting for different lifestages of baroclinic intrusions.

Figure 10 would suggest that warmer 850 hPa temperatures at 20° S and 75° W are correlated to increased subsidence at point Alpha (20° S and 72° W) and near the coast, as is confirmed by the Antofagasta radiosondes. The spatial structure of the 700 hPa subsidence field is further depicted in Fig. 11, and shows that the MAX N_d composite is also characterized by reduced offshore subsidence and a smooth 500 hPa geopotential height wave. In contrast, the MIN- N_d composite has a more developed 500 hPa trough with its axis at 85° W and enhanced offshore subsidence. This pattern is consistent

with the changes in the climatological anticyclone shown in Fig. 6. Perhaps counterintuitively, the increased cloud coverage at 85° W during the MAX- N_d composite is associated with weaker subsidence. While an increased subsidence-decreased cloud fraction relationship is not necessary surprising at short time scales (e.g., Zhang et al., 2009), it does run counter to intuition built from monthly-mean analyses (e.g., Bony and Dufresne, 2005). Figure 11 allows the reduction in subsidence to be interpreted in its larger context, and highlights the meteorological importance of the 850 hPa meridional winds to the southeast Pacific stratocumulus coverage.

Previous studies have associated weaker surface winds at 33° S and 73° W with reduced cold surface temperature advection, in turn reducing cloud liquid water path and cloud fraction north of 20° S (Xu et al., 2004; Muñoz and Garreaud, 2005; Wood et al., 2008). This contrasts with our finding that weaker alongshore winds cooccur with an increase in offshore cloud cover. The explanation may lie in our greater focus on submonthly synoptic activity and analysis of only October months, whereas the previous studies examined longer time spans that probably also captured seasonal changes. Our compositing appears to preferentially select for lifestages of mid-latitude baroclinic waves intruding upon the stratocumulus deck.

Our October 2008 MAX N_d cases ended when a mid-latitude trough moved through the region, while the October 2008 MIN N_d cases loosely coincided with baroclinic troughs (R. Garreaud, 2nd VOCALS Meeting). Warmer temperatures during the MAX N_d composite relative to the MIN N_d composite extend fully throughout the troposphere (not shown), indicating a quasi-barotropic structure with an anomalous anticyclonic circulation. We investigated how this related to other synoptic phenomena besides troughs, in particular the coastal lows and cut-off lows previously documented for this region. The stronger coastal subsidence and slightly stronger coastal easterlies during MAX N_d cases north of 25° S are reminiscent of the shallow, warm-core-low pressure cells of one-three day duration known as coastal lows (e.g., Garreaud et al., 2002; Garreaud and Rutllant, 2003). However, a coastal trough in sea level pressure is not apparent (Fig. 6a), the easterlies at Antofagasta remain weak in comparison to the

Synoptic variability of the stratocumulus deck

D. Painemal and
P. Zuidema

[Title Page](#)[Abstract](#)[Introduction](#)[Conclusions](#)[References](#)[Tables](#)[Figures](#)[⏪](#)[⏩](#)[◀](#)[▶](#)[Back](#)[Close](#)[Full Screen / Esc](#)[Printer-friendly Version](#)[Interactive Discussion](#)

coastal-low easterlies identified in Huneus et al. (2006), and the region south of 25° S is marked by an increase in cloud coverage, rather than a decrease. In addition, although more of our MIN N_d episodes last only one day compared to the MAX N_d cases, the number of episodes lasting three or more days is the same for both composites (five) – longer than for typical coastal low events. Nevertheless, our high/low N_d composites in some ways resemble the ending/leading edge of coastal lows, and the common occurrence of both suggests there must be some common associations.

In contrast to coastal lows, cutoff-lows are upper-level low pressure centers with a quasi-barotropic structure (e.g., Fuenzalida et al., 2005) and thus seem similar to our MIN N_d composite. In addition, cutoff-lows can be preceded by quasi-stationary ridging reminiscent of our MAX N_d composite, with a duration exceeding that of the coastal lows. Cutoff-lows could be considered more intense manifestations of the upper-tropospheric potential vorticity perturbations identified through our composites. Although beyond the scope of the current work, the connection between cut-off lows and our composites seems worthy of further investigation.

5 Precipitation characteristics

We further examined CloudSat radar reflectivities for insight into precipitation impacts on an aerosol budget. Reflectivity-height distributions were constructed for both composites for all Cloudsat data within 17°–27° S and 70°–80° W, an area slightly broader than the Arica Bight. The MAX N_d reflectivity-height distribution is narrower, centered near –25 dBZ and 1000 m, than the MIN N_d distribution (Fig. 12 a and b). For both composites, however, the most frequently occurring reflectivities are around –25 dBZ with heights between 800 m and 1200 m. Few pixels have reflectivities >0 dBZ, equivalent to a cloudbase rain rate of $\sim 2 \text{ mm day}^{-1}$ (Comstock et al., 2004). Approximately one-sixth and one-third of the MAX/MIN N_d pixels exceed –17 dBZ (Table 1), equivalent to a cloudbase rainrate of 0.01 mm day^{-1} . The low radar reflectivities for both composites near the coast can be expected from the thin mean coastal cloud depths

Synoptic variability of the stratocumulus deck

D. Painemal and
P. Zuidema

Title Page

Abstract

Introduction

Conclusions

References

Tables

Figures

⏪

⏩

◀

▶

Back

Close

Full Screen / Esc

Printer-friendly Version

Interactive Discussion



(Fig. 6d, contours). The slightly higher reflectivity values for the MIN N_d distribution are consistent with the deeper clouds and higher cloud tops and do indicate some drizzle, but for the MAX N_d distribution, hypotheses for cloud thinning based on depletion through precipitation seem discouraged (by the lack of observed precipitation).

5 For the coastal clouds, little cloud thinning from precipitation is anticipated, based on a finding that offshore clouds do not become sub-adiabatic until liquid water paths reach $\sim 150 \text{ g/m}^3$ and the frequency of occurrence of cloud radar reflectivities $>0 \text{ dBZ}$ reaches 20% (Zuidema et al., 2005; Fig. 10). This finding will need to be modified for coastal conditions, however, to account for higher N_d and stronger cloud top entrainment.

10 A CloudSat reflectivity-height distribution was also constructed for the offshore region with the most pronounced change in cloud fraction between the two composites, defined by $20^\circ\text{--}30^\circ \text{ S}$ and $80^\circ\text{--}90^\circ \text{ W}$ (Fig. 12c and d). A greater percentage of the offshore pixels are precipitating (reflectivities higher than -17 dBZ), consistent with Leon et al. (2008). The substantial increase in offshore cloud fraction for the MAX N_d composite is associated with only a slight shift towards lower radar reflectivities (Table 1). Fewer of the MAX N_d CloudSat pixels have reflectivities $>-17 \text{ dBZ}$ than the MIN N_d CloudSat pixels, but the discrepancy is less than between the near-shore CloudSat composites. In addition, the percentage of pixels $>0 \text{ dBZ}$ is approximately the same for both offshore composites. Instead, since the N_d difference is small between the two
20 offshore composites, the more pronounced differences in the reflectivity distributions between the near-shore and off-shore composites could be indicative of the impact of aerosols as well as changes in liquid water path (Kubar et al., 2009). In addition, we note the minor change in cloud top height between the offshore MAX and MIN N_d composites, in spite of the large change in large fraction. There is a strong east-west spatial gradient to the cloud top height changes (Fig. 6c), but overall is consistent with some cancelling in the vertical and horizontal temperature advections (i.e. less subsidence
25 but also less free-tropospheric horizontal cold temperature advection).

Synoptic variability of the stratocumulus deck

D. Painemal and
P. Zuidema

[Title Page](#)[Abstract](#)[Introduction](#)[Conclusions](#)[References](#)[Tables](#)[Figures](#)[⏪](#)[⏩](#)[◀](#)[▶](#)[Back](#)[Close](#)[Full Screen / Esc](#)[Printer-friendly Version](#)[Interactive Discussion](#)

6 Conclusions and discussion

We have applied satellite retrievals to understand how synoptic conditions can change cloud droplet number concentrations. We focused on October months only, to reduce influences from the seasonal cycle. Several of the MAX/MIN cases occurred within a day of VOCALS-REx C-130 flights (RF01-03 15–21 October/RF04-RF07 23–28 October, respectively); our analysis can provide context for the VOCALS-REx observations. Comparisons between ship-based and MODIS-derived cloud depth estimates, and of ship-based aerosol concentration to MODIS-derived N_d values establish faith in the satellite retrievals and suggest the aerosol present are readily activated.

Episodes with high N_d over the Arica Bight are associated with a weaker anticyclone, weaker surface and free-tropospheric winds, and thinner clouds, also shown by Wood et al. (2008). We also find higher cloud droplet numbers are associated with more stable atmospheres, similar to Mauger and Norris (2007) and Matsui et al. (2006). In addition, we show that higher N_d values over the Arica Bight are concurrent with lower cloud top heights, consistent with greater subsidence (Fig. 7) and/or a weaker mesoscale convergence in the boundary layer (Zuidema et al., 2009). The horizontal temperature advection reinforces the vertical temperature advection of subsiding, adiabatically-warming air (as deduced from Fig. 10). Smaller differences in N_d occur near 18° S, where the wind speeds are smaller and less variable, allowing aerosols to stagnate. Changes in top-of-atmosphere shortwave fluxes show a spatial gradient, with thinner clouds near the coast dominating a reduction in shortwave reflectance, while 500 km offshore, the increase in cloud droplet number accounts for a slight increase in shortwave reflectance (Fig. 6f). CloudSat cloud radar reflectivity distributions differ between the MAX and MIN N_d composites, with the MAX N_d composite in particular indicating little precipitation (Table 1).

Changes in the easterlies (from radiosondes) at Antofagasta are not higher than 0.5 m s^{-1} between the MAX and MIN N_d composites, and it is doubtful that this modest change can support a significant change in advection of continental aerosols to the Sc

Synoptic variability of the stratocumulus deck

D. Painemal and
P. Zuidema

Title Page

Abstract

Introduction

Conclusions

References

Tables

Figures



Back

Close

Full Screen / Esc

Printer-friendly Version

Interactive Discussion

deck. In addition, the stronger subsidence associated with the higher boundary layer aerosol concentrations will discourage entrainment of free-tropospheric aerosol (Jiang et al., 2002). Rather, the radiosondes suggest that advection of warmer, drier free tropospheric continental air by slightly stronger easterlies during the MAX N_d cases strengthens the cloud top temperature inversion and decreases the boundary layer height. This discourages entrainment and traps aerosols already in the boundary layer, with remaining entrainment promoting cloud thinning (e.g., Ackerman et al., 2004). On a 3–4 day synoptic timescale, the enhanced stability furthers multi-day aerosol transport within the boundary layer from the south, in evidence in Wood et al. (2008), and high N_d conditions can be expected to correlate with enhanced stability from previous days, similar to Mauger and Norris (2007). The aerosol source may then be more likely to be situated in the more developed southern region of Chile, and could include non-point-source pollution from Santiago, Chile (33.3° S and 70.5° W) that has been brought out to sea. Consistent with this, higher aerosol loadings were sampled between 27° S–30° S during VOCALS-REx C130 flights RF11 and RF12 than further north, and in general the highest variability in the cloud droplet concentration is found between 25° S–28° S (Fig. 3). Wind transport appears important for N_d variability.

Approximately one-fourth of potential daily cases were excluded because they did not satisfy our criteria for overcast conditions over the Arica Bight. Given that thinner clouds are associated with the high- N_d composite, the days with low cloud cover over the Arica Bight are more likely to resemble the high- N_d cases. Further south, around 30° S, these days are associated with increased cloud cover, a deeper boundary layer and deeper clouds, and resemble the aftermath of the coastal lows described by Garreaud et al. (2002) and Garreaud and Rutllant (2003). The leading edge of the ~2 day coastal low events encourage conditions conducive to pollution trapping in Santiago, Chile (33.3° S, 70.5° W), as well as easterly winds capable of advecting aerosol-rich air out to sea. The synoptic conditions that encourage coastal lows are similar to those of our MIN N_d composites, though the coastal low troughing in sea level pressure is not as apparent in our composite sea level pressures (Fig. 6b). Coastal lows must un-

Synoptic variability of the stratocumulus deck

D. Painemal and
P. Zuidema

Title Page

Abstract

Introduction

Conclusions

References

Tables

Figures



Back

Close

Full Screen / Esc

Printer-friendly Version

Interactive Discussion

doubtedly impact the southerly manifestation of the high/low N_d composites discussed here.

Huneus et al. (2006) analyzed strong easterly events at Antofagasta (700 hPa zonal winds $>5 \text{ m s}^{-1}$) during austral winter, finding a connection between one episode of upper-level easterlies and the increase of N_d . This suggested a connection to two important copper smelters, Chuquicamata (22.3° S , 68.9° W) and Potrerillos (26.4° S , 69.5° W), that are both above the boundary layer (2700 m and 2850 m a.s.l. respectively). In this study we did not find any event with easterly winds of that magnitude; possibly they are sporadic during austral spring when the midlatitude weather disturbances are less intense.

Further offshore along 85° W , a large increase in cloud fraction and top-of-atmosphere shortwave fluxes is evident in the MAX N_d composite. This is synoptic, driven by mid-latitude baroclinicity rather than from the equator. As revealed in a one-point correlation map (Fig. 10), an anomalously warm 850 hPa temperature near the coast is associated with an offshore trough-like pattern that enhances coastal subsidence but encourages free-tropospheric ascent offshore. The pattern reflects that of an intrusion by a mid-latitude baroclinic wave, rather than an equatorial source. Anomalous northerly winds along 85° W allow the above-inversion temperature to increase and increase the static stability, which is well-correlated with cloud fraction at this location. A similar synoptic episode is discussed in Wyant et al. (2009), but with a reduction of offshore cloud fraction associated with a deeper boundary layer and stronger southerlies. Our more comprehensive analysis indicates that the behavior of the free-tropospheric meridional wind at 85° W is dominant in establishing the southeast Pacific stratocumulus cloud coverage at synoptic timescales. This points to the importance of mid-latitude synoptic intrusions into the subtropical stratocumulus deck, even at 20° S . The 850 hPa meridional winds are a useful meteorological variable to control for when examining this region for cloud-aerosol interactions. It is also useful to note that the changes in cloud cover are counter-intuitive, in that increased cloud cover is associated with decreased subsidence. Yet, as is apparent in Fig. 6, the increased

Synoptic variability of the stratocumulus deck

D. Painemal and
P. Zuidema

Title Page

Abstract

Introduction

Conclusions

References

Tables

Figures

⏪

⏩

◀

▶

Back

Close

Full Screen / Esc

Printer-friendly Version

Interactive Discussion

cloud cover is associated with widespread decreases in cloud top height, because the anomalous horizontal warm temperature advection above the inversion is more than compensating for the decrease in subsidence. The albedo increase from the increase in cloud cover, along with an albedo decrease from near-coastal cloud thinning, means that a spatial gradient in albedo along 20° S will be difficult to detect in some VOCALS-REx aircraft flights.

The most significant features of the circulations associated with the two composites are highlighted in a schematic (Fig. 13).

Several avenues for further work present themselves. The implications of our data for albedo susceptibility $d(A)/d(N_d)$ still need to be assessed. New reanalyses (e.g., Year of Tropical Convection; ERA-Interim; NCEP Climate Forecast System Reanalysis and Reforecast) with better resolution of the orography and of the physical processes will allow for more confident investigations of near-coastal aerosol-cloud interactions. Further investigation of the connection of our composites to the synoptic climatology of the southeast Pacific will also help us better determine the impact of future climates upon this region, arguably the largest subtropical stratocumulus deck on the planet.

Acknowledgements. Funding support from the NOAA Climate Prediction Program for the Americas (Grant NA06OAR4310056) and from the National Science Foundation (Grant ATM-0745470) is gratefully acknowledged.

References

- Ackerman, A., Kirkpatrick, M., Stevens, D., and Toon, O.: The impact of humidity above stratiform clouds on indirect aerosol climate forcing, *Nature*, 432, 1014–1017, 2004.
- Albrecht, B.: Aerosol, clouds microphysics, and fractional cloudiness, *Science*, 245, 1227–1230, 1989.
- Bennartz, R.: Global assessment of marine boundary layer cloud droplet number concentration from satellite, *J. Geophys. Res.*, 112, D02201, doi:10.1029/2006JD007547, 2007.

Synoptic variability of the stratocumulus deck

D. Painemal and
P. Zuidema

Title Page

Abstract

Introduction

Conclusions

References

Tables

Figures

⏪

⏩

◀

▶

Back

Close

Full Screen / Esc

Printer-friendly Version

Interactive Discussion

**Synoptic variability
of the stratocumulus
deck**D. Painemal and
P. Zuidema

[Title Page](#)[Abstract](#)[Introduction](#)[Conclusions](#)[References](#)[Tables](#)[Figures](#)[⏪](#)[⏩](#)[◀](#)[▶](#)[Back](#)[Close](#)[Full Screen / Esc](#)[Printer-friendly Version](#)[Interactive Discussion](#)

- Bony, S. and Dufresne, J.-L.: Marine boundary layer clouds at the heart of tropical cloud feedback uncertainties in climate models, *Geophys. Res. Lett.*, 32, L20806, doi:10.1029/2005GL023851, 2005.
- 5 Borg, L. A. and Bennartz, R.: Vertical structure of stratiform marine boundary layer clouds and its impact on cloud albedo, *Geophys. Res. Lett.*, 34, L05807, doi:10.1029/2006GL028713, 2007.
- Brenguier, J. L., Pawlowska, H., Schüller, L., Preusker, R., Fischer, J., and Fouquart, Y.: Radiative properties of boundary layer clouds: Droplet effective radius versus number concentration, *J. Atmos. Sci.*, 57, 803–821, 2000.
- 10 Brenguier J.-L., Pawlowska, H., and Schüller, L.: Cloud microphysical and radiative properties for parameterization and satellite monitoring of the indirect effect of aerosol on climate, *J. Geophys. Res.*, 108(D15), 8632, doi:10.1029/2002JD002682, 2003.
- Bretherton, C. S., Uttal, T., Fairall, C. W., Yuter, S., Weller, R., Baumgardner, D., Comstock, K., Wood, R., and Raga, G.: The EPIC 2001 stratocumulus study, *B. Am. Meteor. Soc.*, 85, 967–977, 2004.
- 15 Christensen, M. W., Coakley, J. A., and Tahnk, W. R.: Morning-to-Afternoon evolution of marine stratus polluted by underlying ships: Implications for the relative lifetimes of polluted and unpolluted clouds, *J. Atmos. Sci.*, 66, 2097–2106, 2009.
- Comstock, K. K., Wood, R., Yuter, S. E., and Bretherton, C. S.: Reflectivity and rain rate in and below drizzling stratocumulus, *Q. J. Roy. Meteorol. Soc.*, 130, 2891–2918, 2004.
- 20 Comstock, K. K., Bretherton, C. S., and Yuter, S. E.: Mesoscale variability and drizzle in south-east Pacific stratocumulus, *J. Atmos. Sci.*, 62, 3792–3807, 2005.
- Fuenzalida, H. A., Sanchez, R., and Garreaud, R. D.: A climatology of cutoff lows in the Southern Hemisphere, *J. Geophys. Res.*, 110, D18101, doi:10.1029/2005JD005934, 2005.
- 25 Garreaud, R., Rutllant, J., and Fuenzalida, H.: Coastal lows along the subtropical west coast of south America: Mean structure and evolution, *Mon. Weather Rev.*, 130, 75–88, 2002.
- Garreaud, R. and Rutllant, J.: Coastal lows along the subtropical west coast of south America: Numerical simulation of a typical case, *Mon. Weather Rev.*, 131, 891–908, 2003.
- Han, Q., Rossow, W. B., Zeng, J., and Welch, R.: Three different behaviors of liquid water path of water clouds in aerosol-cloud interactions, *J. Atmos. Sci.*, 59, 726–735, 2002.
- 30 Hartmann, D. L., Ockert-Bell, M. E., and Michelsen, M. L.: The effect of cloud type on Earth's balance: Global analysis, *J. Climate*, 5, 1281–1304, 1992.

Hawkins, L. N., Russell, L. M., Covert, D. S., Quinn, P. K., and Bates, T. S.: Carboxylic acids, sulfates, and organosulfates in processed continental organic aerosols over the southeast Pacific ocean during VOCALS-Rex 2008, *J. Geophys. Res.*, submitted, 2009.

5 Huneeus, N., Gallardo, L., and Rutllant, J. A.: Offshore transport episodes of anthropogenic sulfur in northern Chile: Potential impact on the stratocumulus cloud deck, *Geophys. Res. Lett.*, 33, L19819, doi:10.1029/2006GL026921, 2006.

Jiang, H., Feingold, G., and Cotton, W. R.: Simulations of aerosol-cloud-dynamical feedbacks resulting from entrainment of aerosol into the marine boundary layer during the Atlantic Stratocumulus Transition Experiment, *J. Geophys. Res.*, 107(D24), 4813, doi:10.1029/2001JD001502, 2002.

10 Kalnay, E., Kanamitsu, K., Kistler, R., et al: The NCEP/NCAR 40-years Reanalysis project, *B. Am. Meteor. Soc.*, 77, 437–471, 1996.

Kim B.-G., Miller, M. A., Schwartz, S. E., Liu, Y., and Min, Q.: The role of adiabaticity in the aerosol first indirect effect, *J. Geophys. Res.*, 113, D05210, doi:10.1029/2007JD008961, 2008.

Klein, S. A. and Hartmann, D. L.: The seasonal cycle of low stratiform clouds, *J. Climate*, 6, 1587–1606, 1993.

Klein, S. A.: Synoptic variability of low-cloud properties and meteorological parameters in the subtropical trade wind boundary layer, *J. Climate*, 10, 2018–2039, 1997.

20 Kubar, T., Hartmann, D. L., and Wood, R.: Understanding the importance of microphysics for warm rain in marine low clouds: Part I. Satellite observations, *J. Atmos. Sci.*, 66, 2953–2972, 2009.

Leon D. C., Wang, Z., and Liu, D.: Climatology of drizzle in marine boundary layer clouds based on 1 year of data from CloudSat and Cloud-Aerosol Lidar and Infrared Pathfinder Satellite Observations (CALIPSO), *J. Geophys. Res.*, 113, D00A14, doi:10.1029/2008JD009835, 2008.

Loeb, N. and Schuster, G.: An observational study of the relationship between cloud, aerosol and meteorology in broken low-level cloud conditions. *J. Geophys. Res.*, 113, D14214, doi:10.1029/2007JD009763, 2008.

30 Marshak, A., Platnick, S., Varnai, T., Wen, G., and Cahalan, R. F.: Impact of 3D radiative effects on satellite retrievals of cloud droplet sizes. *J. Geophys. Res.*, 111, D09207, doi:10.1029/2005JD006686, 2006.

Matsui, T., Masunaga, H., Kreidenweis, S. M., Pielke Sr., R. A., Tao, W.-K., Chin, M., and

Synoptic variability of the stratocumulus deck

D. Painemal and
P. Zuidema

Title Page

Abstract

Introduction

Conclusions

References

Tables

Figures

◀

▶

◀

▶

Back

Close

Full Screen / Esc

Printer-friendly Version

Interactive Discussion



**Synoptic variability
of the stratocumulus
deck**D. Painemal and
P. Zuidema

Title Page

Abstract

Introduction

Conclusions

References

Tables

Figures

◀

▶

◀

▶

Back

Close

Full Screen / Esc

Printer-friendly Version

Interactive Discussion

Kaufman, Y. J.: Satellite-based assessment of marine low cloud variability associated with aerosol, atmospheric stability, and the diurnal cycle, *J. Geophys. Res.*, 111, D17204, doi:10.1029/2005JD006097, 2006.

5 Mauger, G. S. and Norris, J. R.: Meteorological bias in satellite estimates of aerosol-cloud relationships, *Geophys. Res. Lett.*, 34, L16824, doi:10.1029/2007GL029952, 2007.

McComiskey, A., Feingold, G., Frisch, A. S., Turner, D. D., Miller, M. A., Chiu, J. C., Min, Q., and Ogren, J. A.: An assessment of aerosol-cloud interactions in marine stratus clouds based on surface remote sensing, *J. Geophys. Res.*, 114, D09203, doi:10.1029/2008JD011006, 2009.

10 Muñoz, R. and Garreaud, R.: Dynamics of the low-level jet off the coast of subtropical South America, *Mon. Weather Rev.*, 133, 3661–3677, 2005.

Murphy, D. M., Solomon, S., Portmann, R. W., Roselof, K. H., Forster, P. M., and Wong, T.: An observationally-based energy balance for the Earth system since 1950, *J. Geophys. Res.*, 114, D17107, doi:10.1029/2009JD012105, 2009.

15 Painemal, D., Garreaud, R., Rutllant, J., and Zuidema, P.: Southeast Pacific stratus: High-frequency variability and mesoscale structures over San Felix Island, *J. Appl. Meteor. Climate*, accepted, 2009.

Platnick, S., King, M., Ackerman, S., Menzel, W., Baum, B., Riedi, J., and Frey, R.: The MODIS cloud products: Algorithms and examples from Terra, *IEEE T. Geosci. Remote*, 41, 459–473, 2003.

20 Pruppacher H. R. and Klett, J. D.: *Microphysics of Clouds and Precipitation*, Kluwer Academic, 954 pp., 1997.

Quaas, J., Ming, Y., Menon, S., Takemura, T., Wang, M., Penner, J. E., Gettelman, A., Lohmann, U., Bellouin, N., Boucher, O., Sayer, A. M., Thomas, G. E., McComiskey, A., Feingold, G., Hoose, C., Kristjánsson, J. E., Liu, X., Balkanski, Y., Donner, L. J., Ginoux, P. A., Stier, P., Feichter, J., Sednev, I., Bauer, S. E., Koch, D., Grainger, R. G., Kirkevåg, A., Iversen, T., Seland, Ø., Easter, R., Ghan, S. J., Rasch, P. J., Morrison, H., Lamarque, J.-F., Iacono, M. J., Kinne, S., and Schulz, M.: Aerosol indirect effects – general circulation model intercomparison and evaluation with satellite data, *Atmos. Chem. Phys. Discuss.*, 9, 12731–12779, 2009,

<http://www.atmos-chem-phys-discuss.net/9/12731/2009/>.

30 Schüller, L., Brenguier, J.-L., and Pawlowska, H.: Retrieval of microphysical, geometrical, and radiative properties of marine stratocumulus from remote sensing, *J. Geophys. Res.*,

108(D15), 8631, doi:10.1029/2002JD002680, 2003.

Seethala, C. and Horváth, Á.: Global Assessment of AMSR-E and MODIS Cloud Liquid Water Path Retrievals in Warm Oceanic Clouds, *J. Geophys. Res.*, submitted, 2009.

Stevens, B. and Feingold, G.: Untangling aerosol effects on clouds and precipitation in a buffered system, *Nature*, 461, 607–613, doi:10.1038, 2009.

Szczodrak, M., Austin, P. H., and Krummel, P. B.: Variability of optical depth and effective radius in marine stratocumulus clouds, *J. Atmos. Sci.*, 58, 2912–2926, 2001.

Stephens G. L., Vane, D. G., Boain, R. J., et al.: The CloudSat mission and the A-Train: A new dimension of space-based observations of clouds and precipitation, *B. Am. Meteor. Soc.*, 83, 1771–1790, 2002.

Tomlinson J. M., Li, R., and Collins, D. R.: Physical and chemical properties of the aerosol within the southeastern Pacific marine boundary layer, *J. Geophys. Res.*, 112, D12211, doi:10.1029/2006JD007771, 2007.

Twomey, S.: The influence of pollution on the shortwave albedo of clouds, *J. Atmos. Sci.*, 34, 1149–1152, 1977.

Wielicki, B. A., Barkstrom, B. R., Harrison, E. F., Lee III, R. B., Smith, G. L., and Cooper, J. E.: Clouds and the Earth's Radiant Energy System (CERES): An Earth Observing System Experiment, *B. Am. Meteor. Soc.*, 77, 853–868, 1996.

Wood, R., Comstock, K. K., Bretherton, C. S., Cornish, C., Tomlinson, J., Collins, D. R., and Fairall, C.: Open cellular structure in marine stratocumulus sheets, *J. Geophys. Res.*, 113, D12207, doi:10.1029/2007JD009371, 2008.

Wood, R. and Mechoso, C. R.: Southeastern Pacific Coupled Climate Field Experiment, *EOS, Transactions American Geophysical Union*, 89(33), 303, doi:10.1029/2008EO330003, 2008.

Wyant, M. C., Wood, R., Bretherton, C. S., Mechoso, C. R., Bacmeister, J., Balmaseda, M. A., Barrett, B., Codron, F., Earnshaw, P., Fast, J., Hannay, C., Kaiser, J. W., Kitagawa, H., Klein, S. A., Khler, M., Manganello, J., Pan, H.-L., Sun, F., Wang, S., and Wang, Y.: The PreVOCA experiment: modeling the lower troposphere in the Southeast Pacific, *Atmos. Chem. Phys. Discuss.*, 9, 23909–23953, 2009, <http://www.atmos-chem-phys-discuss.net/9/23909/2009/>.

Xu, H., Wang, Y., and Xie, S.-P.: Effects of the Andes on eastern Pacific climate: A regional atmospheric model study, *J. Climate*, 17, 589–602, 2004.

Zhang, Y., Stevens, B., Medeiros, B., and Ghil, M.: Low-cloud fraction, lower-tropospheric stability and large-scale subsidence, *J. Climate*, 22, 4827–4844, 2009.

ACPD

9, 25523–25564, 2009

Synoptic variability of the stratocumulus deck

D. Painemal and
P. Zuidema

Title Page

Abstract

Introduction

Conclusions

References

Tables

Figures

◀

▶

◀

▶

Back

Close

Full Screen / Esc

Printer-friendly Version

Interactive Discussion

Zuidema, P., Westwater, E., Fairall, C., and Hazen, D.: Ship-based liquid water path estimates in marine stratocumulus, *J. Geophys. Res.*, 110, D20206, doi:10.1029/2005JD005833, 2005.
Zuidema, P., Painemal, D., de Szoeki, S., and Fairall, C.: Stratocumulus cloud top height estimates and their climatic implications, *J. Climate*, 22, 4652–4666, 2009.

ACPD

9, 25523–25564, 2009

**Synoptic variability
of the stratocumulus
deck**

D. Painemal and
P. Zuidema

Title Page

Abstract

Introduction

Conclusions

References

Tables

Figures

◀

▶

◀

▶

Back

Close

Full Screen / Esc

Printer-friendly Version

Interactive Discussion

25550



Synoptic variability of the stratocumulus deck

D. Painemal and
P. Zuidema

Table 1. Number and percentage of CloudSat pixels below two km of height, at two separate regions, above two different reflectivity thresholds.

	Domain	$\text{dBZ} \geq -17$	$\text{dBZ} > 0$
MAX N_d	17°–27° S and 70°–80° W	973 pixels/13.6%	44 pixels/0.6%
MIN N_d	17°–27° S and 70°–80° W	13 611 pixels/37.4%	1168 pixels/3.2%
MAX N_d	20°–30° S and 80°–90° W	11 596 pixels/43.9%	2589 pixels/9.8%
MIN N_d	20°–30° S and 80°–90° W	26 006 pixels/55.4%	4013 pixels/8.5%

[Title Page](#)
[Abstract](#)
[Introduction](#)
[Conclusions](#)
[References](#)
[Tables](#)
[Figures](#)
[Back](#)
[Close](#)
[Full Screen / Esc](#)
[Printer-friendly Version](#)
[Interactive Discussion](#)

Synoptic variability of the stratocumulus deck

D. Painemal and
P. Zuidema

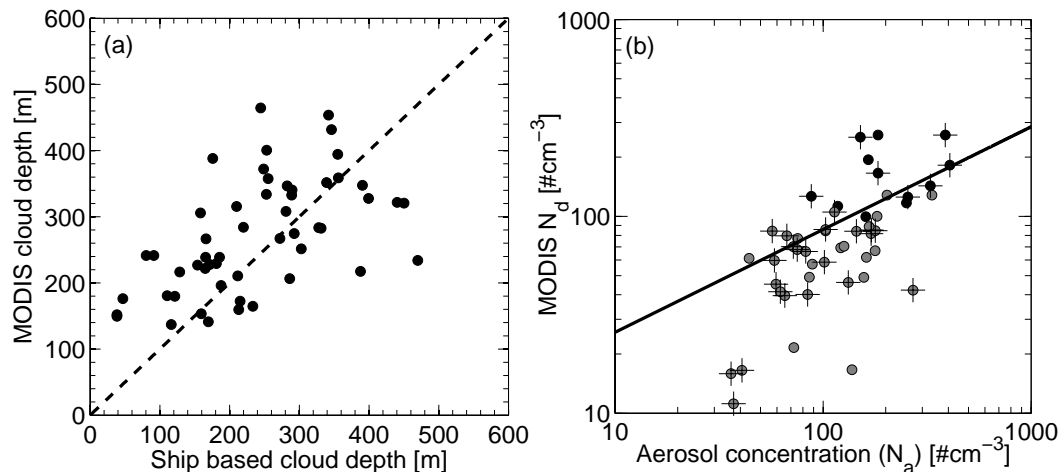


Fig. 1. (a) MODIS-derived cloud depth versus ship-based cloud depth (hourly averaged; ceilometer cloud fraction >0.9), and (b) MODIS-derived N_d versus ship-based accumulation-mode ($r > 0.1$ mm) aerosol concentrations (hourly-averaged; no restriction on ceilometer cloud fraction). Black dots indicate samples east of 80° W and crosses are samples for which the bias-corrected MODIS H_{sat} is within 70 m of H_{ship} . The black solid line represents the best-fit line for all values with $N_d > 50$ cm⁻³. Sampling domain covers 0° – 30° S, 72° W– 90° W. (a) and (b) were constructed with 51 and 48 samples, respectively.

[Title Page](#)[Abstract](#)[Introduction](#)[Conclusions](#)[References](#)[Tables](#)[Figures](#)[◀](#)[▶](#)[◀](#)[▶](#)[Back](#)[Close](#)[Full Screen / Esc](#)[Printer-friendly Version](#)[Interactive Discussion](#)

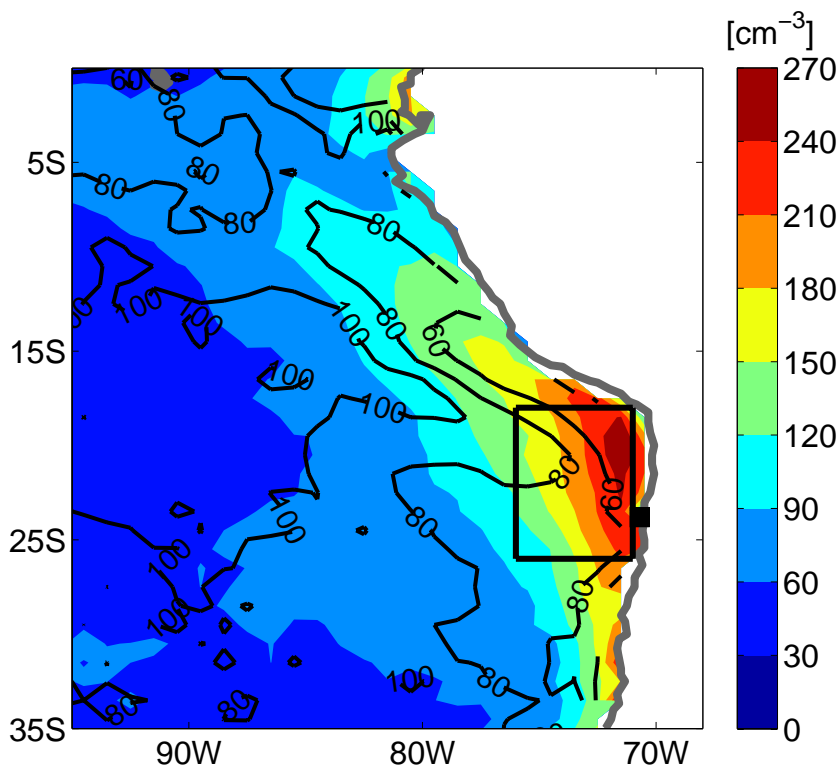
**Synoptic variability
of the stratocumulus
deck**D. Painemal and
P. Zuidema

Fig. 2. Mean N_d ($\# \text{ cm}^{-3}$, colors) and LWP (g m^{-2} , contours), based on October 2001 and 2005–2008 Terra daytime MODIS level 3 data. The box indicates the area over which the daily-mean N_d were averaged and the black square indicates Antofagasta.

[Title Page](#)[Abstract](#)[Introduction](#)[Conclusions](#)[References](#)[Tables](#)[Figures](#)[◀](#)[▶](#)[◀](#)[▶](#)[Back](#)[Close](#)[Full Screen / Esc](#)[Printer-friendly Version](#)[Interactive Discussion](#)

Synoptic variability of the stratocumulus deck

D. Painemal and
P. Zuidema

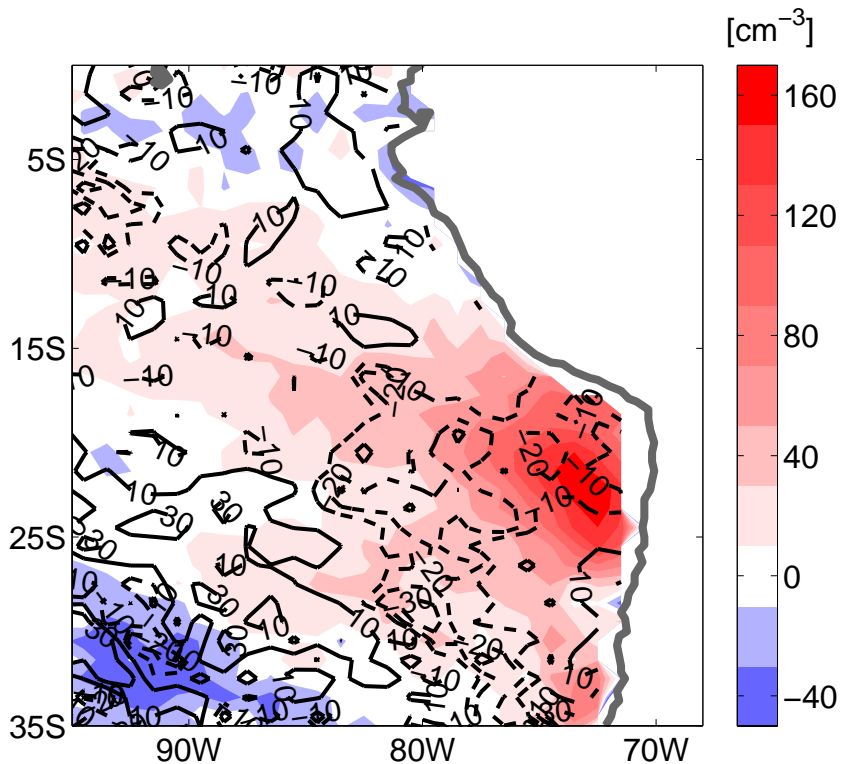


Fig. 3. As Fig. 2 but for the MAX-MIN N_d composite differences: N_d (colors) and LWP (contours).

[Title Page](#)[Abstract](#)[Introduction](#)[Conclusions](#)[References](#)[Tables](#)[Figures](#)[◀](#)[▶](#)[◀](#)[▶](#)[Back](#)[Close](#)[Full Screen / Esc](#)[Printer-friendly Version](#)[Interactive Discussion](#)

Synoptic variability of the stratocumulus deck

D. Painemal and
P. Zuidema

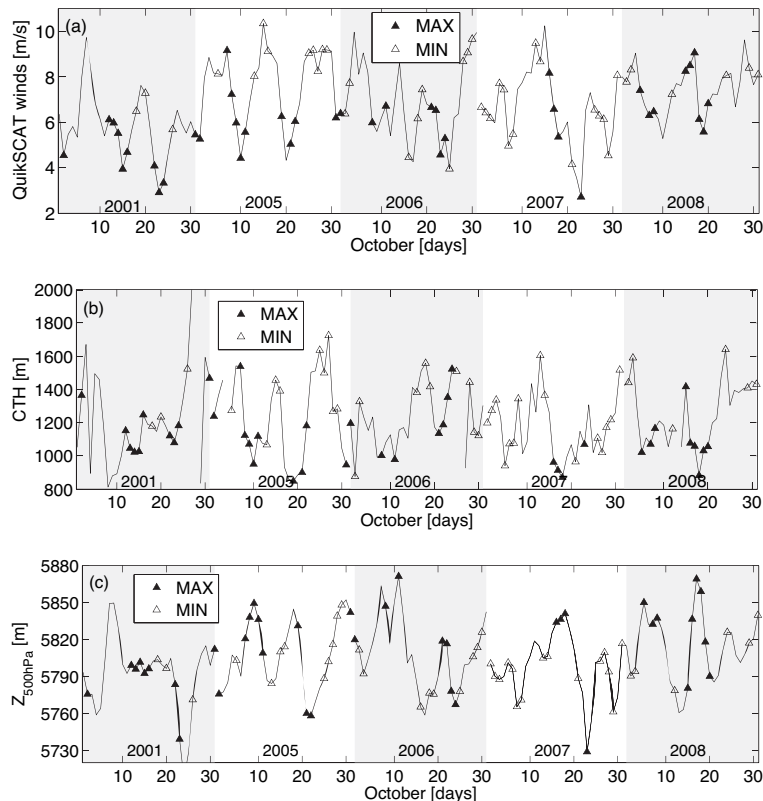


Fig. 4. Time series of: **(a)** mean surface winds (QuikSCAT) at 20°S – 30°S , 70°W – 100°W , **(b)** mean Terra-daytime MODIS-derived cloud top heights at 20°S – 30°S , 70°W – 80°W and **(c)** mean 500 hPa geopotential height at 15°S – 35°S , 70°W – 100°W . Black and open triangles correspond to MAX and MIN N_d days.

[Title Page](#)[Abstract](#)[Introduction](#)[Conclusions](#)[References](#)[Tables](#)[Figures](#)[◀](#)[▶](#)[◀](#)[▶](#)[Back](#)[Close](#)[Full Screen / Esc](#)[Printer-friendly Version](#)[Interactive Discussion](#)

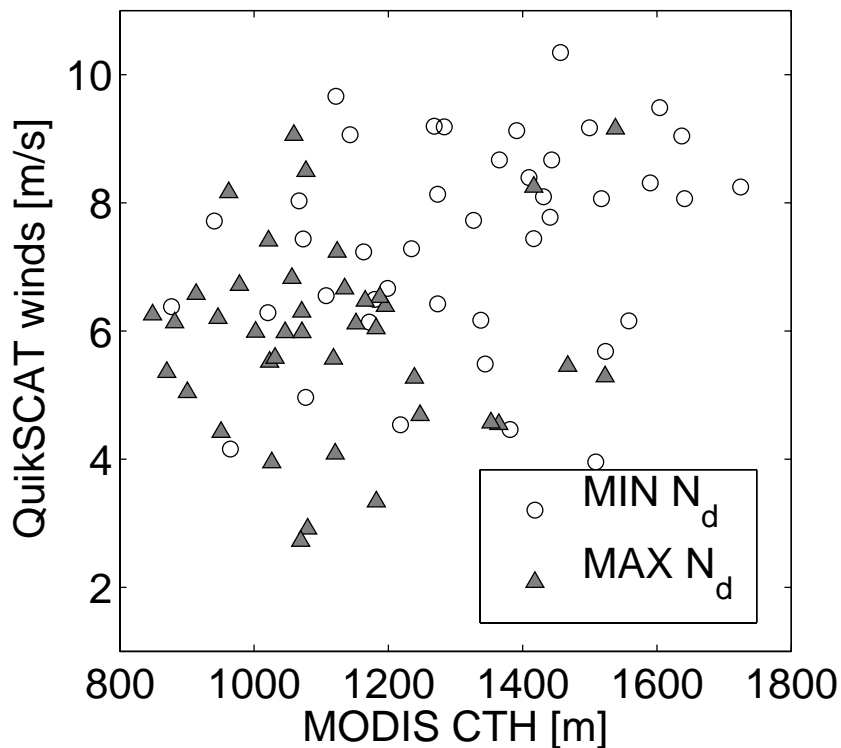
**Synoptic variability
of the stratocumulus
deck**D. Painemal and
P. Zuidema

Fig. 5. Scatterplot between Terra daytime MODIS-derived cloud top height and evening-pass QuikSCAT winds, taken from Fig. 4. Open circles and filled triangles correspond to MIN and MAX N_d days, respectively.

[Title Page](#)[Abstract](#)[Introduction](#)[Conclusions](#)[References](#)[Tables](#)[Figures](#)[◀](#)[▶](#)[◀](#)[▶](#)[Back](#)[Close](#)[Full Screen / Esc](#)[Printer-friendly Version](#)[Interactive Discussion](#)

Synoptic variability of the stratocumulus deck

D. Painemal and
P. Zuidema

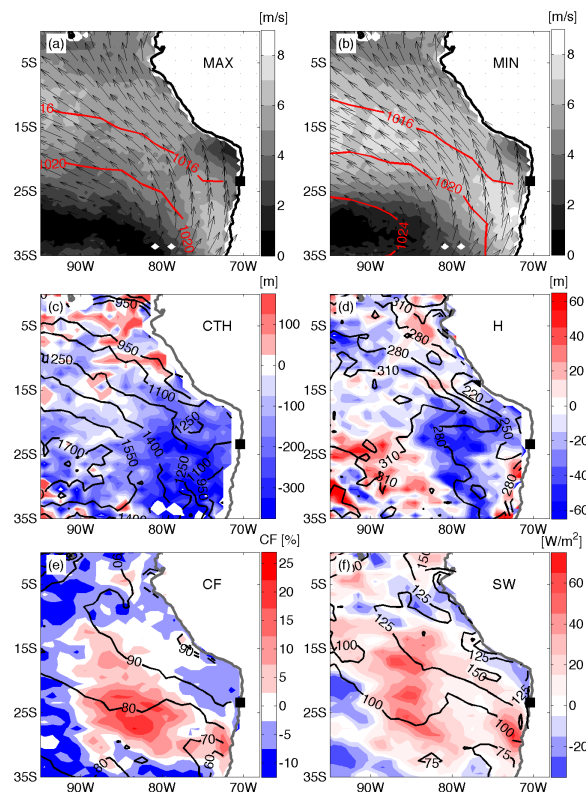


Fig. 6. (a) and (b) MAX and MIN N_d composite NCEP sea level pressure (red contours), surface wind magnitude and direction (greyscale and arrows; QuikSCAT descending pass, 18:00 LT). Mean (contours) and MAX-MIN composite difference (colors) in (c) MODIS-derived cloud top height, (d) MODIS-derived cloud depth, (e) MODIS cloud fraction and (f) CERES top-of-atmosphere shortwave fluxes. All MODIS data is Terra daytime level 3. Location of Antofagasta indicated by black square.

[Title Page](#)
[Abstract](#)
[Introduction](#)
[Conclusions](#)
[References](#)
[Tables](#)
[Figures](#)
[◀](#)
[▶](#)
[◀](#)
[▶](#)
[Back](#)
[Close](#)
[Full Screen / Esc](#)
[Printer-friendly Version](#)
[Interactive Discussion](#)

Synoptic variability of the stratocumulus deck

D. Painemal and
P. Zuidema

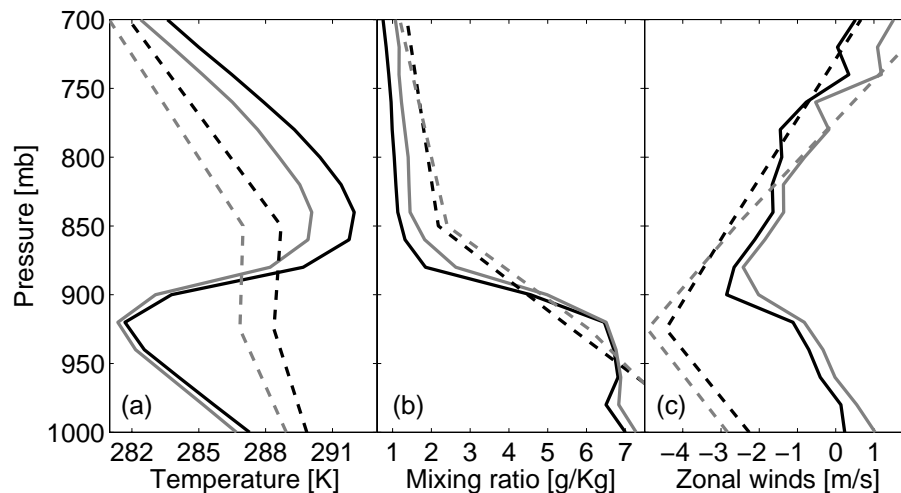


Fig. 7. Antofagasta radiosonde (solid) and NCEP reanalysis (dashed) MAX (black) and MIN (grey) composites of **(a)** temperature, **(b)** mixing ratio, and **(c)** zonal winds. Antofagasta (23.5° S, 70.5° W) radiosondes launched at 12:00 UTC (08:00 LT). NCEP-NCAR reanalysis data from 22.5° S, 75° W.

[Title Page](#)[Abstract](#)[Introduction](#)[Conclusions](#)[References](#)[Tables](#)[Figures](#)[◀](#)[▶](#)[◀](#)[▶](#)[Back](#)[Close](#)[Full Screen / Esc](#)[Printer-friendly Version](#)[Interactive Discussion](#)

Synoptic variability of the stratocumulus deck

D. Painemal and
P. Zuidema

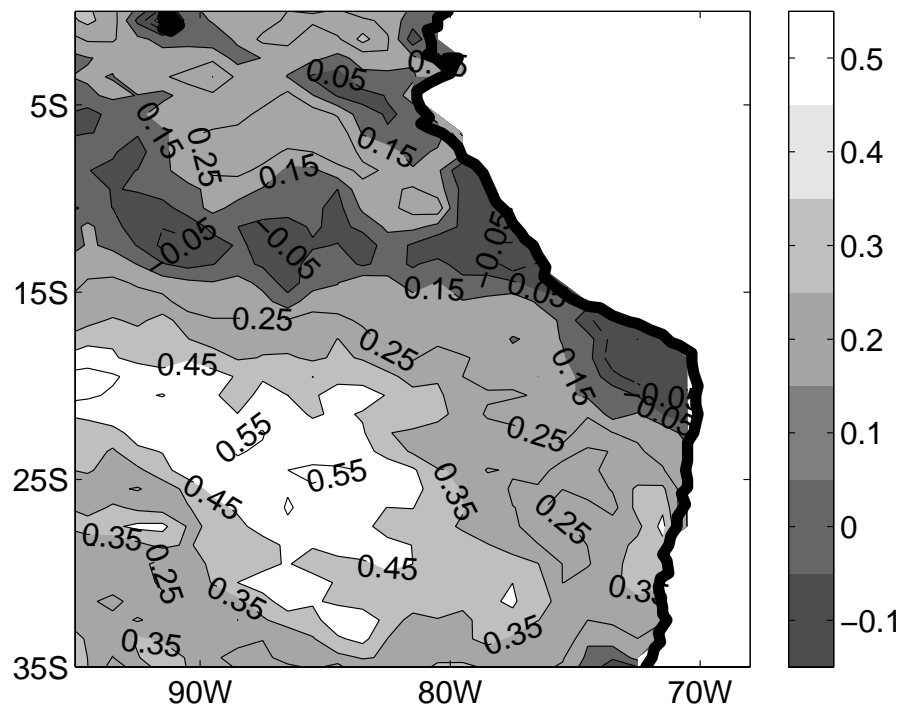


Fig. 8. Linear correlation between daytime Terra MODIS cloud fraction and daily-mean $\theta_{850\text{hPa}} - \theta_{1000\text{hPa}}$. Correlation values greater than 0.20 below 15°S pass the 99% significance level of a Student's *t* test.

[Title Page](#)[Abstract](#)[Introduction](#)[Conclusions](#)[References](#)[Tables](#)[Figures](#)[◀](#)[▶](#)[◀](#)[▶](#)[Back](#)[Close](#)[Full Screen / Esc](#)[Printer-friendly Version](#)[Interactive Discussion](#)

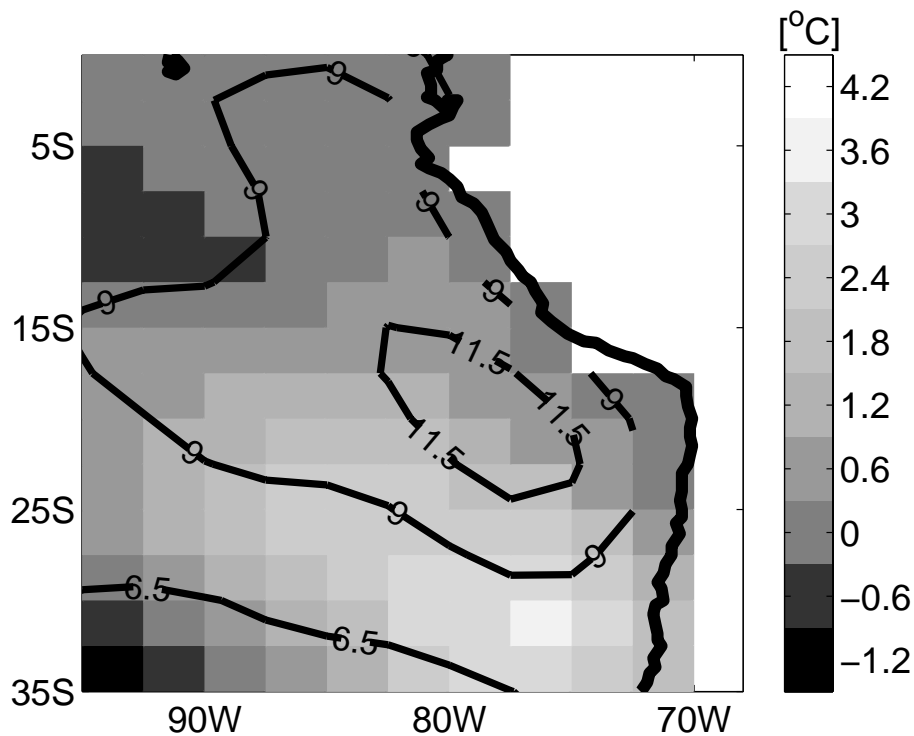
**Synoptic variability
of the stratocumulus
deck**D. Painemal and
P. Zuidema

Fig. 9. October-mean $\theta_{850\text{hPa}} - \theta_{1000\text{hPa}}$ (contours) and MAX-MIN N_d composite differences in $\theta_{850\text{hPa}} - \theta_{1000\text{hPa}}$ (greyscale).

[Title Page](#)[Abstract](#)[Introduction](#)[Conclusions](#)[References](#)[Tables](#)[Figures](#)[◀](#)[▶](#)[◀](#)[▶](#)[Back](#)[Close](#)[Full Screen / Esc](#)[Printer-friendly Version](#)[Interactive Discussion](#)

Synoptic variability of the stratocumulus deck

D. Painemal and
P. Zuidema

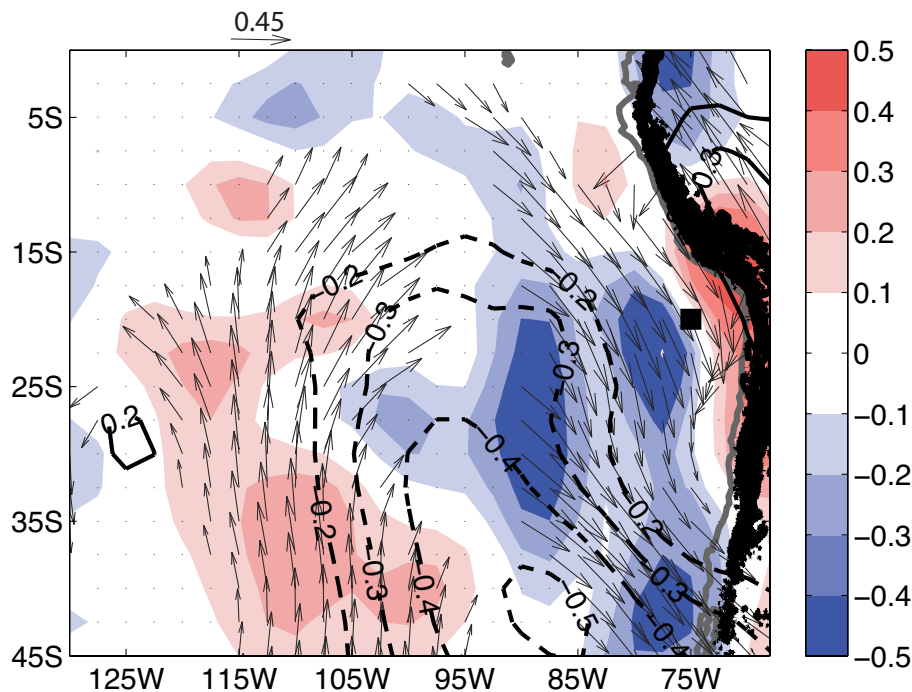


Fig. 10. One point correlation between the 850 hPa temperature at 20° S and 75° W (square) and: subsidence (pressure velocity dp/dt , colors; positive values imply subsidence), geopotential height (contours) and wind (arrows), all at 850 hPa. Absolute values of correlation higher than 0.25 for the geopotential height and subsidence fields pass the 99% significance level of a Student's *t* test. The winds are only shown if the meridional component of the wind-temperature correlation is statistically significant. Topography higher than 1500 m is indicated by the black shade.

Title Page

Abstract

Introduction

Conclusions

References

Tables

Figures

◀

▶

◀

▶

Back

Close

Full Screen / Esc

Printer-friendly Version

Interactive Discussion

Synoptic variability of the stratocumulus deck

D. Painemal and
P. Zuidema

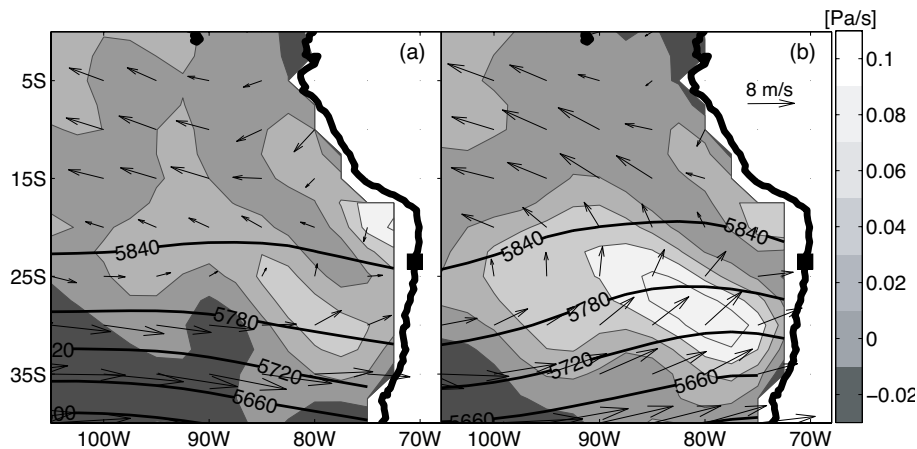


Fig. 11. NCEP reanalysis geopotential heights (contours) at 500 hPa, 700 hPa subsidence (dp/dt , greyscale), and 700 hPa winds, for (a) MAX N_d composite, (b) MIN N_d composite. Antofagasta location indicated with an open black box.

Title Page

Abstract

Introduction

Conclusions

References

Tables

Figures

◀

▶

◀

▶

Back

Close

Full Screen / Esc

Printer-friendly Version

Interactive Discussion

Synoptic variability of the stratocumulus deck

D. Painemal and
P. Zuidema

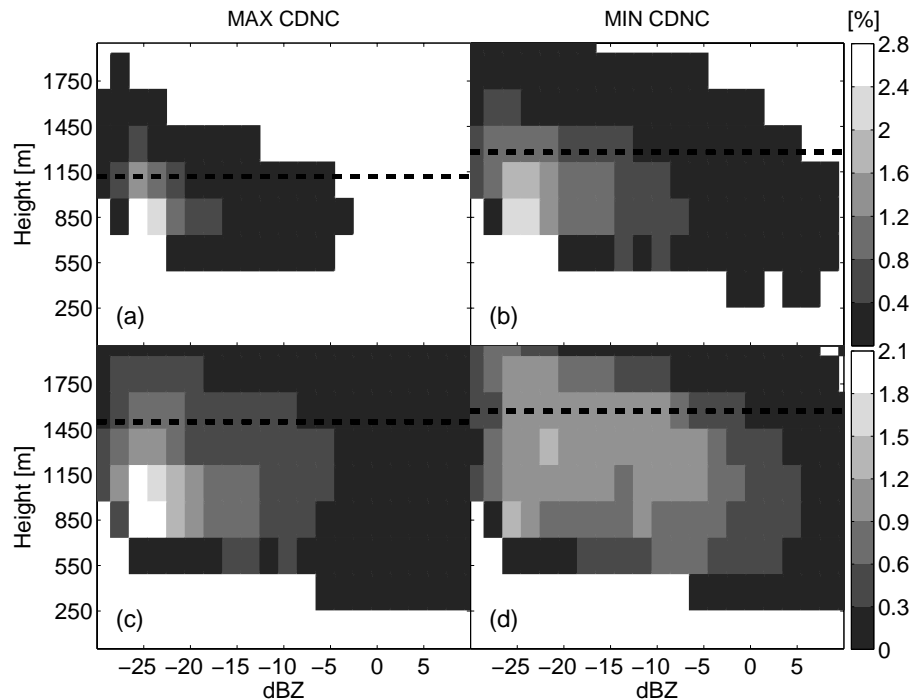


Fig. 12. CloudSat reflectivity-height distributions for 17° S–27° S and 70° W–80° W **(a)** MAX N_d , **(b)** MIN N_d ,; and 20° S–30° S and 80° W–90° W **(c)** MAX N_d , **(d)** MIN N_d . The colors indicate the percentage of the total pixels at each altitude; their summation over reflectivity equals total cloud fraction at that altitude. The dashed line indicates mean MODIS-derived cloud top height.

Title Page

Abstract

Introduction

Conclusions

References

Tables

Figures

◀

▶

◀

▶

Back

Close

Full Screen / Esc

Printer-friendly Version

Interactive Discussion

Synoptic variability of the stratocumulus deck

D. Painemal and
P. Zuidema

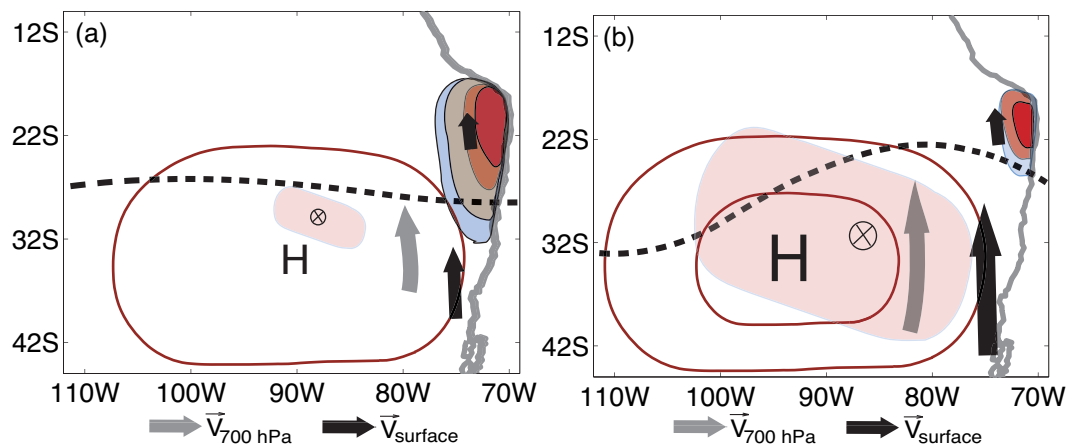


Fig. 13. Schematic of (a) MAX N_d , and (b) MIN N_d large-scale meteorology. The 500 hPa geopotential height is indicated by the dashed line, the sea-level pressure by red contours, subsidence by the shaded area, 700 hPa and surface winds by grey and black arrows, respectively.

Title Page

Abstract

Introduction

Conclusions

References

Tables

Figures

◀

▶

◀

▶

Back

Close

Full Screen / Esc

Printer-friendly Version

Interactive Discussion